

Stripe Structures in the t - t' - J Model

D.J. Scalapino

Physics Department, University of California, Santa Barbara, CA 93106-9530, USA

S.R. White

Physics Department, University of California, Irvine, CA 92697, USA

Abstract

Here, based upon density matrix renormalization group calculations, we discuss the structure of the stripes found in the doped t - t' - J model and the physics that underlies their formation.

Keywords:

t - t' - J , stripes, DMRG

1. Introduction

From the variety of experiments described in this review issue, it is clear that stripes, or stripe-like fluctuations, appear as groundstates or important low-energy configurations in the underdoped cuprates. Furthermore, in the presence of impurities or lattice defects, the interplay between randomness and the stripe-like correlations can lead to the electronic inhomogeneity observed in these materials at low doping [1]. There have been various theoretical models and explanations for the occurrence of these stripes. Early on, Hartree-Fock calculations [2–5] for the doped Hubbard model found that one-dimensional domains of increased hole density forming anti-phase Néel

boundaries were present in the mean-field solutions. Here, the stability of the stripe structure arose from the reduction in the kinetic energy that the holes experienced in moving transverse to the stripes. The stripes in this Hartree-Fock solution were insulating, characterized by a filling of one hole per domain wall unit cell, while experiments on the cuprates found a filling of half this [6]. An alternate view proposed that stripes could arise from a competition between phase separation and long-range Coulomb interactions [7]. In this “frustrated phase separation” approach, it was argued that lightly doped t - J and Hubbard models would, in the absence of a long-range Coulomb interaction, globally phase separate into uniform hole-rich and undoped regions. While there are disagreements regarding whether the simple two-dimensional t - J or Hubbard models, with parameters in the relevant physical regime, will in fact exhibit phase separation, if phase separation occurs, the formation of stripes in this scenario depends upon the suppression of the phase separation by the long-range Coulomb interaction. In this case, the stripes can be metallic. In a third scenario, which we will discuss, the formation of stripes in the 2D t - J model is found to involve, in addition to the reduction of kinetic energy of the holes arising from the π -phase shifted antiferromagnetic stripe correlations, d -wave pairing correlations leading to half-filled stripes [8, 9].

In the following, we will review density matrix renormalization group [10] (DMRG) results for the t - J model. The Hamiltonian for the basic t - J model is

$$H = -t \sum_{\langle ij \rangle s} (c_{is}^\dagger c_{js} + \text{h.c.}) + J \sum_{\langle ij \rangle} \left(\mathbf{S}_i \cdot \mathbf{S}_j - \frac{n_i n_j}{4} \right) \quad (1)$$

Here $\langle ij \rangle$ are nearest-neighbor sites, s is a spin index and doubly occupied

sites are explicitly excluded from the Hilbert space. The operator c_{is}^\dagger creates an electron of spin s on site i and $\mathbf{S}_i = \frac{1}{2}c_{is}^\dagger \boldsymbol{\sigma} c_{is}$ and $n_i = c_{i\uparrow}^\dagger c_{i\uparrow} + c_{i\downarrow}^\dagger c_{i\downarrow}$ are the electron spin moment and charge density operators at site i . The nearest-neighbor hopping and exchange interaction are t and J , respectively, and the average site occupation $\langle n \rangle = 1 - x$ is set by the hole doping parameter x . A next-near-neighbor hopping t' will also be considered. Except for cases in which a proximity pairfield is applied, the particle number will be fixed.

2. DMRG Results for the t - J Model

Figure 1 shows DMRG results for the central 8×8 section of a 16×8

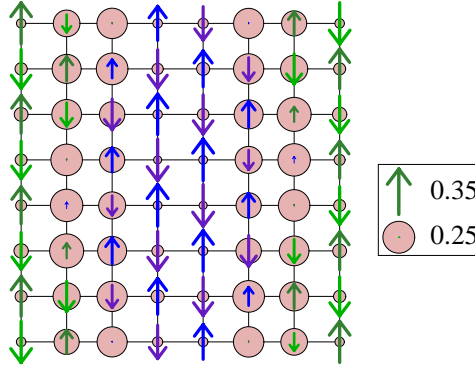


Figure 1: Hole density and spin moments on a center section of a 16×8 $t - J$ lattice with $J/t = 0.35$ and an average hole density $x = 0.125$. The diameter of the circles is proportional to the hole density $\langle n_i \rangle$ on the i th site and the length of the arrows is proportional to $\langle S_i^z \rangle$ according to the scales shown. The arrows are color coded to show different antiferromagnetic domains. This structure depends on the boundary conditions as discussed in the text. (From [8].)

lattice which has periodic boundary conditions in the y -direction and open

end boundary conditions in the x -direction forming an open ended cylinder. Here, $J/t = 0.35$ and there are 16 holes corresponding to a doping $x = 1/8$. Along the left and right ends of the cylinder a small staggered magnetic field of magnitude $h = 0.1t$ was applied. This field breaks the spin symmetry and the open ends break the translational symmetry in the x -direction, giving rise to nonhomogeneous finite values of the hole occupation $\langle n_i \rangle$ and spin $\langle S_i^z \rangle$. The basic pattern consists of domain walls containing excess hole density separated by π -phase shifted antiferromagnetic regions. There are four holes per domain wall, and as we will discuss this linear filling of 0.5 holes per unit length of the domain wall is the preferred filling. Here the boundary conditions only act to pin the stripes and calculations with different boundary conditions provide evidence that the basic stripe pattern is intrinsic.

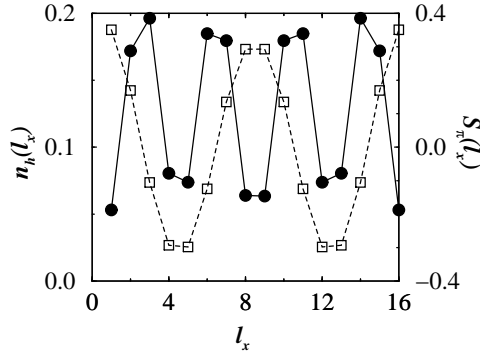


Figure 2: Average hole density $n_h(\ell_x)$ (solid circles) and spin structure function $S_\pi(\ell_x)$ (open squares) versus ℓ_x for the 16×8 system of Fig. 1. [11]

A more detailed look at the domain wall structure is shown in Fig. 2.

Here the ℓ_x dependence of the average hole density

$$n_h(\ell_x) = \frac{1}{L_y} \sum_{\ell_y=1}^{L_y} \left(1 - \left\langle c_{\ell_x \ell_y \uparrow}^\dagger c_{\ell_x \ell_y \uparrow} + c_{\ell_x \ell_y \downarrow}^\dagger c_{\ell_x \ell_y \downarrow} \right\rangle \right) \quad (2)$$

and the spin structure

$$S_\pi(\ell_x) = \frac{1}{L_y} \sum_{\ell_y=1}^{L_y} (-1)^{\ell_x + \ell_y} \langle S^z(\ell_x, \ell_y) \rangle \quad (3)$$

are shown as a function of the x -coordinate ℓ_x . The charge structure of these domain walls is evident as is the π -phase shifted antiferromagnetic regions separating them.

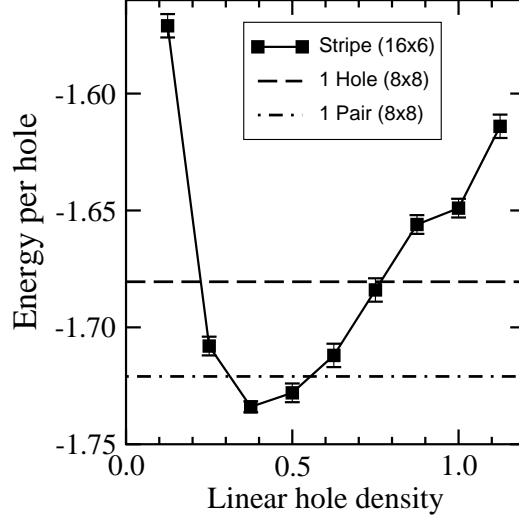


Figure 3: Energy per hole for a 16×6 stripe versus the linear density of holes ρ_ℓ . The horizontal lines mark the energy per hole of one hole (dashed line) and two holes (dot-dashed line) placed on an open 8×8 lattice with a staggered field of magnitude 0.1 on all four sides [12].

In Fig. 3, we show the energy per hole as a function of the linear hole density ρ_ℓ measured on a 16×6 system with open end boundary conditions

and with a staggered π -phase shifted magnetic field of magnitude $h = 0.1$ applied to the top and bottom rows of sites. There is a minimum for a linear density $\rho_\ell \sim 0.5$. The dashed line on this plot shows the energy of one hole on an 8×8 lattice with a staggered field of magnitude 0.1 on all four sides while the dash-dot line is the energy per hole of two holes on this lattice. The fact that the energy per hole of two holes is lower than that of a single hole indicates that two holes pair in agreement with exact diagonalization studies. However, we note that the energy per hole associated with the domain wall for $\rho_\ell \sim 0.5$ is even lower suggesting that pairs condense into domain walls even at low doping. The interaction between domain walls was also studied and was found to be repulsive.

Thus for $x \lesssim 0.125$, $\rho_\ell \sim 0.5$ (1,0) domain walls are favored and their spacing d is equal to $(2x)^{-1}$. For $x \gtrsim 0.17$, the DMRG calculations find $\rho_\ell \simeq 1$ domain walls begin to form. At this filling the energy per hole for the (1,0) and (1,1) walls, as well as the pairs, are nearly degenerate leading to large fluctuations in the configurations [12].

In addition to the charge and spin structure of the domains, they also exhibit an underlying pairfield structure which can be described in terms of the near neighbor pairfield operators

$$\Delta_x^\dagger(\ell_x, \ell_y) = \frac{1}{\sqrt{2}} \left(c_\uparrow^\dagger(\ell_x + 1, \ell_y) c_\downarrow^\dagger(\ell_x, \ell_y) - c_\downarrow^\dagger(\ell_x + 1, \ell_y) c_\uparrow^\dagger(\ell_x, \ell_y) \right) \quad (4)$$

and

$$\Delta_y^\dagger(\ell_x, \ell_y) = \frac{1}{\sqrt{2}} \left(c_\uparrow^\dagger(\ell_x, \ell_y + 1) c_\downarrow^\dagger(\ell_x, \ell_y) - c_\downarrow^\dagger(\ell_x, \ell_y + 1) c_\uparrow^\dagger(\ell_x, \ell_y) \right) \quad (5)$$

The first term creates a singlet pair on the $(\ell_x + 1, \ell_y) - (\ell_x, \ell_y)$ link of the lattice and the second term creates a pair on a corresponding y -link.

Since the stripes have broken the C_4 rotational symmetry of the lattice, the pairfield-pairfield correlations for x -link pairs differ from those of the y -link pairs. However, the d -wave-like nature of the pairing correlations is evident in the fact that $\langle \Delta_y(\ell'_x, \ell'_y) \Delta_x^\dagger(\ell_x, \ell_y) \rangle$ is found to be negative[9].

Based on the behavior of the two-leg t - J ladder [13, 14], it is natural to expect that the stripes will exhibit pairfield correlations. For the two-leg ladder, one knows that these correlations have a power law decay and indeed if a sufficient number of states are kept in the DMRG calculations, a power law decay is observed. However, the off diagonal nature of the pairing correlations makes this one of the more challenging calculations.

In addition, for the striped systems of interest, there are further difficulties. Consider the 16×8 lattice shown in Fig. 1, where the boundary conditions are such that the stripes run around the circumference of the cylinder with each stripe on average containing 4 holes corresponding to a linear hole density $\rho = 0.5$. Fluctuations in which a pair of holes is exchanged between two of the stripes leaving one stripe with 2 holes and another with 6 holes lead to linear hole densities of 0.25 and 0.75, respectively in the two stripes. From Fig. 3, one can see that such large deviations of the linear hole density are energetically costly so that pair number fluctuations are suppressed leading in turn to the suppression of the pairfield correlations. In order to study longer stripes which can more readily support density fluctuations, we have considered systems which have slightly anisotropic exchange interactions ($J_x = 0.55$, $J_y = 0.45$)[9]. As shown in Fig. 4a, this anisotropy favors stripes that are oriented along the long x -axis of a 12×8 cylinder. Here, in addition to the magnetic fields, a proximity pairfield cou-

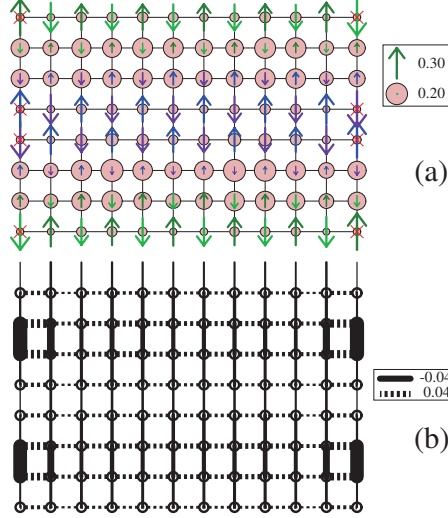


Figure 4: (a) A 12×18 t - J lattice with cylindrical boundary conditions in the y -direction with $J_x = 0.55$, $J_y = 0.45$ such that the stripes run along the x -axis. Here we have applied a magnetic field $h = \pm 0.2$ on the sites with a red X, and a pair field $\Delta_0 = 1.0$ to the edge links without X's. A chemical potential $\mu = 1.23$ was used to give a doping of $x = 0.127$. (b) The pair field strength $\langle \Delta_\alpha^\dagger(\ell_x, \ell_y) + \Delta_\alpha(\ell_x, \ell_y) \rangle$ on the $\alpha = x$ and y links for the system shown in (a) [9].

pling $\Delta_0(\ell_x, \ell_y) (\Delta_y^\dagger(\ell_x, \ell_y) + \Delta_y(\ell_x, \ell_y))$ was applied to rungs at both ends of the cylinder. In the presence of this proximity pairfield, the total number of electrons is only conserved modulo two, and a chemical potential μ was introduced to control the average number of holes.

Figure 4b shows the expectation value of the proximity induced pair-field $\langle \Delta_\alpha^\dagger(\ell_x, \ell_y) + \Delta_\alpha(\ell_x, \ell_y) \rangle$ for $\alpha = x$ and y with a coupling strength $\Delta_0(\ell_x, \ell_y) = 1$ for the four thickest end links and 0.5 for the four vertical links adjacent to them. The d -wave-like sign changes of the induced pair-field are clearly seen in Fig. 4b. If the proximity pairfield is applied to the

end rungs of only one of the domains, the structure of the induced pairfield pattern remains similar, but the amplitude of the induced pairfield on the domain that is not coupled to the proximity pairfield becomes considerably weaker. This again reflects the fact that it is energetically unfavorable for the number of hole pairs in a domain of this length which is not coupled to an external pair reservoir to have significant hole number fluctuations.

As seen in Fig. 4b, the proximity pairfield induces a pairfield which spreads out over the lattice but decays in strength as one moves away from the source. In order to look in more detail at this induced pairfield, it is useful to separate questions dealing with pairing on a stripe and pairing between stripes. For the first question, we have studied a single stripe on the 5×16 lattice with cylindrical periodic boundary conditions shown in Fig. 5a. In this case, the periodic boundary conditions in the cylindrical direction give rise to one stripe, similar to those shown in Fig. 1. Then, applying a proximity pairfield to only one end of the stripe one obtains the induced pairfield shown in Fig. 5b. The strength of the induced pairfield depends upon J , the next near neighbor hopping t' and the doping x . As previously found in various numerical calculations [15, 16], a positive value of t' favors pairing while a negative value suppresses it. Figure 6 shows the rung and leg induced pairfields $\langle \Delta_x^\dagger(3, \ell_y) + \Delta_x(3, \ell_y) \rangle$ and $\langle \Delta_y^\dagger(3, \ell_y) + \Delta_y(3, \ell_y) \rangle$ versus ℓ_y for a linear filling $\rho_\ell = 0.5$ for $J = 0.5$ and $t' = 0$ and 0.2 . The d -wave-like character of the pairfield is evident. The magnitude of the induced pairfield on the 12th $x = 3$ -4 rung is shown in Fig. 7 versus the linear hole doping ρ_ℓ . When the pairing is strongest, the response peaks for $\rho_\ell \sim 0.5$ holes per unit length.

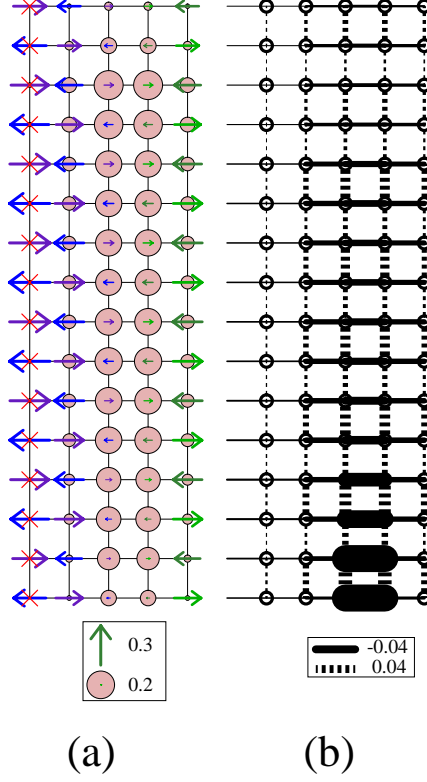


Figure 5: A single forced stripe on a 5×16 lattice with cylindrical boundary conditions. Here, $J = 0.5$ and $t' = 0.2$. On the $x = 5$ leg, a staggered field $(-1)^y h$ with $h = 0.05$ was applied, along with a chemical potential of 2.0. On the other 4 legs, a chemical potential μ was applied to vary the doping. In the case shown $\mu = 1.41$, yielding a doping of $x = 0.106$, which corresponds to a linear doping of 0.53. In each case a strong pair field was applied to four rungs ($y = 1$ to 4, connecting $x = 3$ and $x = 4$), visible as the four thickest links in (b). The magnitude of the applied field on the four rungs was 1.0, 1.0, 0.5, 0.25. (a) The hole density $\langle 1 - n_i \rangle$ and spin density $\langle S_i^z \rangle$. (b) The measured pair field $\langle \Delta_\alpha^\dagger(\ell_x, \ell_y) + \Delta_\alpha(\ell_x, \ell_y) \rangle$ [9].

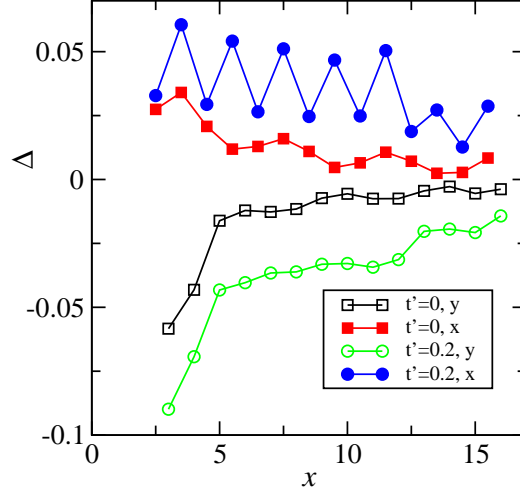


Figure 6: The 3–4 rung $\langle \Delta_x^\dagger(3, \ell_y) + \Delta_x(3, \ell_y) \rangle$ and the third leg $\langle \Delta_y^\dagger(3, \ell_y) + \Delta_y(3, \ell_y) \rangle$ induced pairfields versus ℓ_y for the 5×16 lattice of Fig. 5.

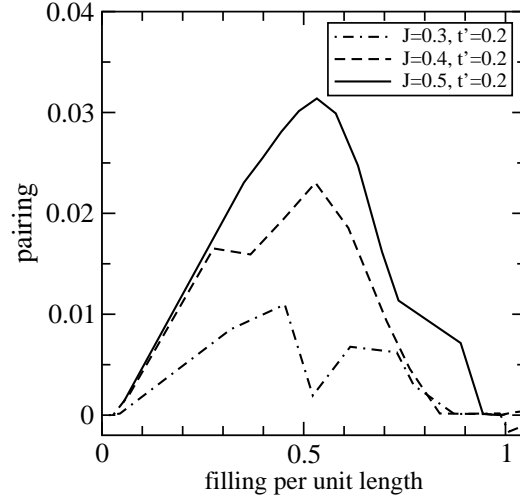


Figure 7: The measured pair field at the $y = 12$, $x = 3$ –4 rung versus the number of holes per unit length [9].

The second question involving the nature of the pairing between stripes was studied using a 6×12 lattice with open boundary conditions in both the x

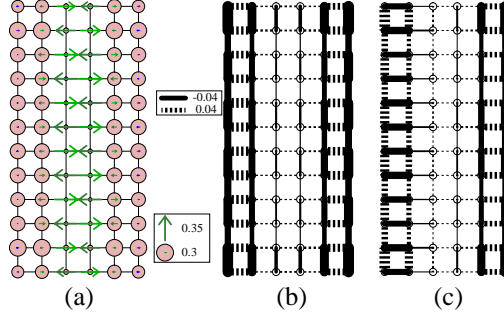


Figure 8: (a) Hole and spin densities for a 6×12 lattice with $J = 0.5$ and $t' = 0$, and with open boundary conditions in both directions with fields applied to force two stripes. The center two legs have an applied staggered field $(-1)^y h$ with $h = 0.05$, along with a chemical potential of 1.3. The outer four legs have a chemical potential of 0.9, leading to a doping of $x = 0.1981$, corresponding to a linear doping per stripe of 0.594. The outermost two legs have applied pair fields of 0.5 on each vertical rung. In (a), the pair fields are applied in phase. (b) Measured pair fields for the in-phase case. (c) Measured pair fields when the applied fields have opposite sign [9].

and y directions. In this case, external magnetic and chemical potential fields were used to force two stripes to form as shown in Fig. 8a. Then the pairfield response was studied when an external proximity pairfield was applied to the vertical links on the outermost ($x = 1$ and 6) legs. In Fig. 8b, the applied proximity pairfields were in phase and in case Fig. 8c they were out of phase. For t' negative the DMRG calculations found that energy difference between the relative pair phase of the two domain walls was negligible, consistent with the weak overall pairfield response found for $t' < 0$. For $t' = 0.0$ and 0.2, the energy to form an antiphase d -wave domain wall was found to be small but positive [9], of order 5% of the energy difference per hole between one hole and a pair shown in Fig. 5 for $t' = 0.2$. A similar conclusion was reached in

renormalized mean field theory calculations [17]. Nevertheless, the difference in energy between the in phase and antiphase d -wave pairfield states is small and there have been various suggestions [18], approximations [19], and model calculations [20, 21] which find that the antiphase pairing state can have the lowest energy.

The picture that emerges from these DMRG calculations for the t - J model is that for dopings $x \lesssim 0.125$, (1,0) domain walls are favored. These walls have a linear hole filling $\rho_\ell = 0.5$ and repel each other, leading to a domain wall spacing $d = (2x)^{-1}$. The structure of the domain wall consists of a stripe-like region of excess holes several lattice spacings in width surrounded by antiferromagnetic regions with fewer holes which are π -phase shifted across the stripe. The domain walls also have short range d -wave-like pairfield correlations. A proximity pairfield applied to one domain creates a d -wave-like response which extends in phase over a neighboring domain, but appears within the present calculation to be short range. Depending upon the boundary conditions, it is also possible to have site-centered domain walls. The minimum energy filling remains $\rho_\ell = 0.5$ and there are similar d -wave pairfield correlations. In general, the stripes tend to occupy more than one column or row so that there is not a sharp distinction between site- and bond-centered stripes, and intermediate centerings are possible.

3. Physical mechanism

In this section, we seek to determine the nature of the physics that underlies the properties of the domain walls which have been described in Sec. 2.

To begin, there is of course the question of phase separation. Emery

[23] et al. originally argued that the 2D t - J model phase separates for all J/t interaction strengths close to half filling. Hellberg and Manousakis [24], using a Green's function Monte Carlo technique, found results that supported this. However, Calandra et al. [25], who also used Green's function Monte Carlo, concluded that phase separation only occurred if $J/t > 0.4$ and Putikka [26] et al., using a high temperature series expansion, concluded that phase separation for dopings near half-filling required $J/t > 1.2$.

The DMRG is known to be most effective for one-dimensional systems and ladder systems of limited width. Therefore, we have studied the phase separation question by examining a sequence of ladders which have an increasing number of legs. For these n -leg ladders with n up to 6, the DMRG results provide reliable results for the $\langle n \rangle - J/t$ phase separation boundary.

In a t - J ladder with two or more legs, the phase-separated system consists of one region containing holes and one region without any holes. An example of this for a 4-leg ladder is shown in Fig. 9. For a given value of J/t and hole doping x , the average number of holes per site $\langle n_h \rangle$ in the hole-rich region determines a point on the phase boundary between the phase separated and uniform systems. Some DMRG results for the phase separation boundary showing $\langle n_e \rangle = 1 - \langle n_h \rangle$ versus J/t for ladders with up to six legs are given in Fig. 10a. In the absence of an exact functional form for the convergence to 2D, we have plotted linear and quadratic fits to the inverse number of legs in Fig. 10b. It appears from these results that the 2D system is away from the phase separation boundary for physically relevant J/t values and we believe that the ground state of the 2D t - J model at small J/t , close to half filling, will be striped and not phase separated. For the present discussion,

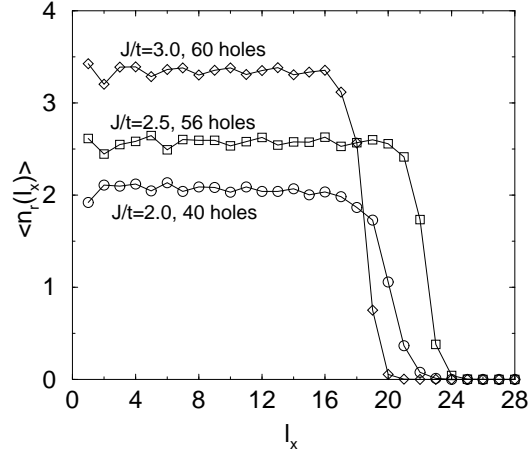


Figure 9: Density of holes on the rungs of a 4×28 system for three different values of J/t , all of which allow phase separation [22].

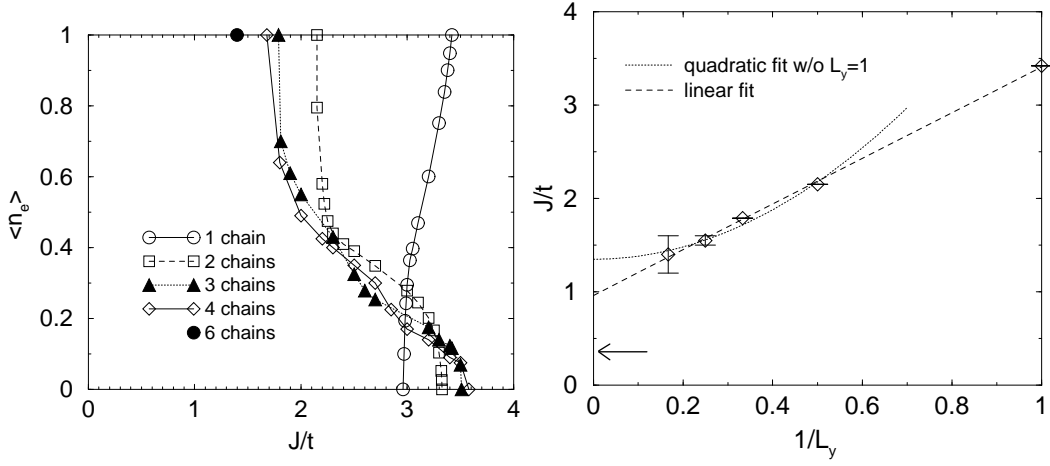


Figure 10: Left panel: Boundary to phase separated region where $\langle n_e \rangle$ is the total electron density of the system. Phase separation is realized to the right of the curves. Right panel: Phase separation boundary at low hole doping as a function of the inverse number of legs. The arrow indicates $J/t \approx 0.35$, a typical value of J/t for the cuprates [22].

the important point is that calculations on lattices we have discussed show no evidence of phase separation in the J/t parameter regimes of interest.

Next, there are the spin correlations whose π -phase shift across the stripe are known to play an essential role in the Hartree-Fock solutions [2–5]. Here it is useful to introduce an operator

$$\mathbb{P}(\ell_1, \ell_2, \dots, \ell_m) = \prod_{i=1}^m p(\ell_i) \quad (6)$$

with $p(\ell) = (1 - n_{\ell\uparrow})(1 - n_{\ell\downarrow})$ the hole projection operator for the ℓ th lattice site. The operator \mathbb{P} projects out a part of the groundstate that has m holes located at sites $\ell_1, \ell_2, \dots, \ell_m$. One can then separate the wavefunction $|\psi\rangle$ into parts which have specific hole locations

$$|\psi\rangle = \sum_{\{\ell_i\}} \mathbb{P}(\ell_i) |\psi\rangle = \sum_{\{\ell_i\}} a(\ell_i) |\psi_{\{\ell_i\}}\rangle \quad (7)$$

Here, $|\psi_{\ell}\rangle$ is a normalized wave function with holes at specific sites and $a(\ell_i) > 0$. Using the DMRG, one can study $|\psi_{\{\ell_i\}}\rangle$ directly and then from it evaluate various expectation values [27]. We will focus on the expectation value of $\mathbf{S}_i \cdot \mathbf{S}_j$. This measurement gives one a “snapshot” of the $\langle \mathbf{S}_i \cdot \mathbf{S}_j \rangle$ configuration associated with a given hole configuration. We will use the term “antiferromagnetic bond” or just “bond” to indicate that $\langle \mathbf{S}_i \cdot \mathbf{S}_j \rangle < 0$. If this expectation value is close to -0.75 for two sites i and j , one would say that there is a “singlet bond” connecting i and j , even if there is no term in the Hamiltonian directly coupling i and j .

Using this projection technique, the spin configuration associated with the domain structure of Fig. 1 is shown in Fig. 11. The blue circles show the most probable configuration of the eight holes on the 8×8 section shown

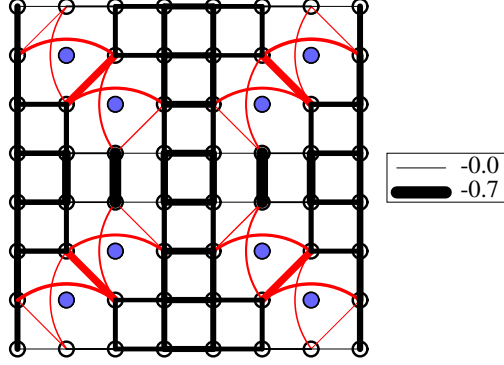


Figure 11: For an 8×8 system with $x = 0.125$ whose hole density and spin patterns are similar to that shown in Fig. 1, the blue dots show the most probable configuration of all the holes and the strength of the exchange bonds $|\langle \mathbf{S}_i \cdot \mathbf{S}_j \rangle|$ between two sites is denoted by the thickness of the line connecting the sites. Anomalous antiferromagnetic correlations across holes are colored red. Only correlations where $\langle \mathbf{S}_i \cdot \mathbf{S}_j \rangle < 0$ are shown [8].

in Fig. 1. The thickness of the lines connecting various sites denotes the strength of the exchange field $\langle \mathbf{S}_i \cdot \mathbf{S}_j \rangle$ for this configuration of the holes.

In Fig. 11 one sees that exchange bonds form across the mobile holes. This reflects the local competition between the kinetic and exchange energies. The domain wall allows most of the exchange bonds to form in a way which cooperates, rather than competes, with the background spin configuration. In particular, the domain wall forms to support π phase-shifted antiferromagnetic regions on either side to reduce the disturbance of the exchange interactions and to lower the transverse kinetic energy of the holes. This is the basic physics that underlies the Hartree-Fock results.

However, as we have seen, the domain walls are also characterized by d -wave pairfield correlations. To see how these correlations are reflected in Fig. 11, we examine this projection for a single pair. Two of the “most prob-

able” hole and spin configurations associated with the groundstate of a pair of holes on an 8×8 lattice with $J/t = 0.35$ and a staggered AF ($h = 0.1$) boundary field are illustrated in Fig. 12. Here, as before, the holes are shown

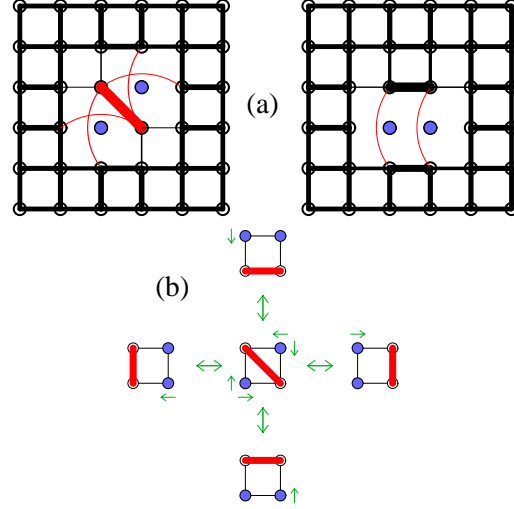


Figure 12: (a) The two most probable hole configurations and associated local exchange field $\langle \mathbf{S}_i \cdot \mathbf{S}_j \rangle$ correlations in the two hole ground state of the system shown in Fig. 11. The scale and conventions are the same as in Fig. 11, but only the central 6×6 region is shown. (b) Schematic illustration showing the one-electron hops from the diagonal configurations which lead to the low energy configurations and contribute to a lowering of the kinetic energy [8].

as blue dots and the thickness of the solid lines denote the singlet bond strength between sites. In the right panel, the holes sit on adjacent sites and this configuration corresponds to what one would expect when the exchange J is large compared with the hopping t . In this case, the holes occupy neighboring sites to reduce the number of broken exchange interactions. However, in the physical regime with an exchange J that is small compared with the hopping t , the dynamics is important and the configuration shown in the left

panel of Fig. 12 is more probable.

This bound pair of holes is characterized by a 2×2 core region and to better understand it we consider the 2×2 lattice shown in Fig. 12b. Using the near neighbor singlet pair operator between sites i and j ,

$$\Delta_{ij}^\dagger = \frac{1}{\sqrt{2}}(c_{i\uparrow}^\dagger c_{j\downarrow}^\dagger - c_{i\downarrow}^\dagger c_{j\uparrow}^\dagger) \quad (8)$$

one can write the groundstate of the undoped half-filled system as

$$|\psi\rangle_0 = N_0[\Delta_{14}^\dagger \Delta_{23}^\dagger - \Delta_{12}^\dagger \Delta_{34}^\dagger]|0\rangle \quad (9)$$

with $|0\rangle$ the vacuum. The groundstate of the two-hole system is

$$|\psi\rangle_2 = N_2 \left[a \left(\Delta_{12}^\dagger + \Delta_{23}^\dagger + \Delta_{34}^\dagger + \Delta_{14}^\dagger \right) + b \left(\Delta_{13}^\dagger + \Delta_{24}^\dagger \right) \right] |0\rangle \quad (10)$$

with $a = 1$ and $b = \left(2 + \left(\frac{J}{4t} \right)^2 \right)^{1/2} - \left(\frac{J}{4t} \right)$. Then in the doped, two-hole state $|\psi\rangle_2$, the ratio of the near-neighbor singlet to the diagonal singlet amplitude is

$$\frac{a}{b} = \frac{1}{\left[2 + \left(\frac{J}{4t} \right)^2 \right]^{1/2} - \frac{J}{4t}} \quad (11)$$

For $J/t = 2$, this ratio is unity. For $J/t < 2$, the diagonal amplitude is larger than the edge amplitude. This is reflected in the t - J results previously discussed, where the hole-hole correlations were found to be larger for next-nearest-neighbor diagonal sites than for nearest-neighbor sites.

The groundstate, Eq. (9), of the undoped 2×2 system transforms as $d_{x^2-y^2}$, while the two-hole state, Eq. (10), transforms as an s -wave. Thus, the hole-pair creation operator that connects $|\psi\rangle_0$ to $|\psi\rangle_2$ must transform as $d_{x^2-y^2}$ [28, 29]. A simple nearest-neighbor operator of this form is

$$\Delta = \Delta_{14} - \Delta_{12} + \Delta_{23} - \Delta_{34}. \quad (12)$$

Applying this to the undoped groundstate $|\psi\rangle_0$ given by Eq. (9), one finds that

$$\Delta|\psi\rangle_0 = -2N_0[\Delta_{12}^\dagger + \Delta_{23}^\dagger + \Delta_{34}^\dagger + \Delta_{14}^\dagger]|0\rangle, \quad (13)$$

which clearly has a nonzero overlap with the two-hole groundstate $|\psi\rangle_2$.

A $d_{x^2-y^2}$ hole pair creation operator, generalized to include holes on next-nearest-neighbor diagonal sites, has been discussed by Poilblanc [30]. One can expand a generalized hole-pair creation operator in terms of operators which create a pair of holes on sites separated by a distance R . For our 2×2 cluster, this involves

$$\Delta_{d_{x^2-y^2}} = \sum_R \Delta_R, \quad (14)$$

with $R = 1$ and $R = \sqrt{2}$. The nearest-neighbor operator Δ_1 is just the operator given in Eq. (12) and a next-nearest-neighbor term possessing $d_{x^2-y^2}$ symmetry [30] is

$$\Delta_{\sqrt{2}} = (\mathbf{S}_1 - \mathbf{S}_3) \cdot \mathbf{T}_{24} - (\mathbf{S}_2 - \mathbf{S}_4) \cdot \mathbf{T}_{31}, \quad (15)$$

with

$$\mathbf{S}_1 \cdot \mathbf{T}_{24} = \frac{1}{2}(c_{1\uparrow}^\dagger c_{1\uparrow} - c_{1\downarrow}^\dagger c_{1\downarrow})(c_{2\uparrow} c_{4\downarrow} - c_{4\uparrow} c_{2\downarrow}) + c_{1\uparrow}^\dagger c_{1\downarrow} c_{2\uparrow} c_{4\uparrow} + c_{1\downarrow}^\dagger c_{1\uparrow} c_{2\downarrow} c_{4\downarrow}. \quad (16)$$

Note that since $\mathbf{T}_{24} = -\mathbf{T}_{42}$, Eq. (15) has $d_{x^2-y^2}$ symmetry. Acting on the undoped groundstate, $\Delta_{\sqrt{2}}$ generates the diagonal singlets

$$\Delta_{\sqrt{2}}|\psi\rangle_0 \sim (\Delta_{13}^\dagger + \Delta_{24}^\dagger)|0\rangle. \quad (17)$$

Thus, the projection studies of the patterns of the probable hole locations and the exchange field $\langle \mathbf{S}_i \cdot \mathbf{S}_j \rangle$ strength show that the stripes contain hole and spin structures which have similar features to that of a d -wave pair.

4. Conclusions

The domain wall structures found in doped t - J lattices consist of relatively narrow (1,0) stripes containing excess holes surrounded by more lightly doped π phase shifted antiferromagnetic regions. The linear hole density $\rho_\ell = 0.5$ along a stripe corresponds to one hole per domain wall unit cell and the stripes repel each other. This leads to a stripe spacing $d = (2x)^{-1}$ for a doping in which the average number of electrons per site $\langle n_e \rangle = 1 - x$. For dopings larger than $x \sim 0.17$, the domain walls cease to appear as well defined structures.

In addition to the charge and spin structures which appear in the domain walls, the application of a proximity pairfield on the boundary of a domain produces a d -wave-like pairfield response. For the parameter range we have studied, the induced pairfield extends over the system without an alternation in its overall phase but appears to be short range. Examination of the “most probable” hole configurations and the exchange field $\langle \mathbf{S}_i \cdot \mathbf{S}_j \rangle$ structures associated with these configurations show patterns which reflect the presence of d -wave pairing correlations in the domain walls. Hartree-Fock calculations which neglect these pairfield correlations give insulating domain walls with $\rho_\ell = 1.0$. Thus, the pairing correlations are an important feature of the striped phase found in the t - J model.

DMRG calculations also find evidence for similar stripes in the Hubbard model [31, 32]. In addition, dynamic cluster quantum Monte Carlo simulations of a 2D Hubbard model with imposed stripe-like charge-density-wave modulations find that the strength of the pairing correlations depend upon both the amplitude and wave vector of the charge modulation[33]. The fact

that both the t - J and Hubbard models exhibit such domain wall structures provides support for the belief that these models contain important parts of the basic physics associated with the high T_c cuprates.

Nevertheless, there are some striking experimental results which remain to be understood. For example [34], the co-doped super-oxygenated $\text{La}_{2-x}\text{Sr}_x\text{CuO}_{4+y}$ exhibits both a long-range incommensurate antiferromagnetic phase with $\langle n_h \rangle \simeq 0.125$ and a superconducting phase with $\langle n_h \rangle \simeq 0.16$. It appears that this material phase separates into two line compounds having different hole densities but with $T_N \simeq T_s \simeq 40\text{K}$. In $\text{La}_2\text{CuO}_{4.11}$, which has interstitial oxygen positioned in every fourth La_2O_2 layer, spin-stripe and bulk superconductivity appear simultaneously at $T_c = 42\text{K}$ [35]. Finally, anisotropic transport and magnetization data for $\text{La}_{1.875}\text{Ba}_{0.125}\text{CuO}_4$ provide evidence that two-dimensional superconducting correlations coexist with the stripe order up to temperatures of order 40K [36]. The absence of 3D superconducting order above $T_c \sim 4\text{K}$ suggests an antiphase ordering in the superconducting state which could then suppress the interlayer Josephson coupling.

As noted, there are models [20, 22] that can give rise to such intertwined phases and early variational Monte Carlo calculations [19] found that for $t' < 0$ stripe states with antiphase d -wave superconducting order were in fact stabilized relative to stripes with in-phase superconductivity. However, both the DMRG calculations that we have discussed and recent renormalized mean-field theory calculations [17] find that the antiphase d -wave state is slightly higher in energy than that of the in-phase state. Thus, while it appears that the t - t' - J models provide a good starting point for discussing stripes, there remains more to be understood.

Acknowledgments

DJS acknowledges the support of the Center for Nanophase Materials Science at ORNL which is sponsored by the Division of Science User Facilities, U.S. DOE. SRW would like to thank the NSF for support under DMR 090-7500.

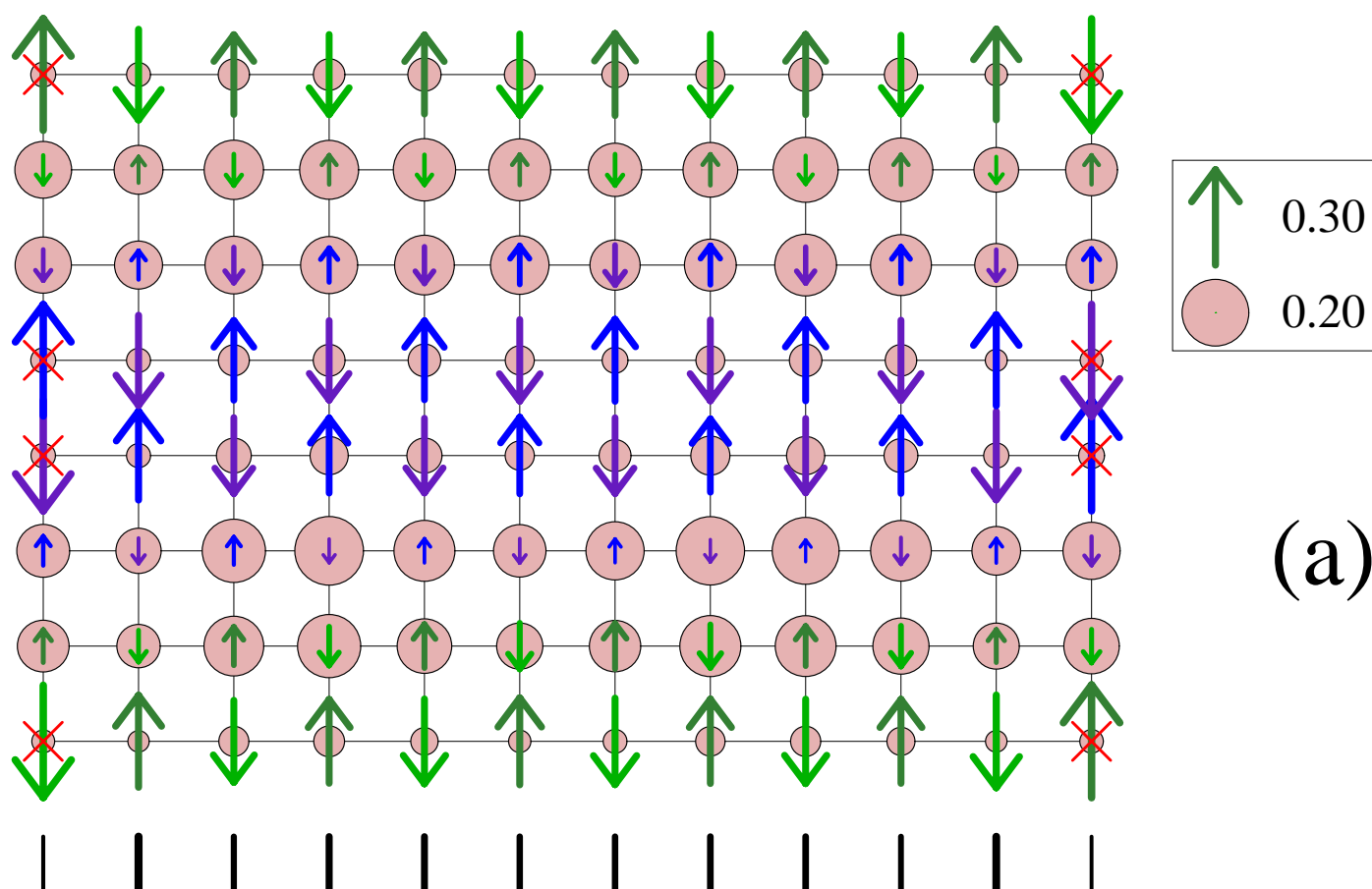
References

- [1] S.A. Kivelson, I.P. Bindloss, E. Fradkin, V. Oganessian, J.M. Tranquada, A. Kapitulnik, and C. Howald, *Rev. Mod. Phys.* **75**, 1201 (2003).
- [2] D. Poilblanc and T.M. Rice, *Phys. Rev. B* **39**, 9749 (1989)
- [3] J. Zaanen and O. Gunnarsson, *Phys. Rev. B* **40**, 7391 (1989)
- [4] K. Machida, *Physica (Amsterdam)* **158C**, 192 (1989).
- [5] H.J. Schultz, *Phys. Rev. Lett.* **64**, 1445 (1990)
- [6] J.M. Tranquada et al., *Nature* **429**, 534 (2004)
- [7] V.J. Emery and S.A. Kivelson, *Physica C* **209**, 597 (1993); S.A. Kivelson and V.J. Emery, p.619 in Proc. “Strongly Correlated Electronic Materials; The Los Alamos Symposium 1993”, K.S. Bedell et al., eds. (Addison Wesley, Redwood City, CA, 1994)
- [8] S.R. White and D.J. Scalapino, “Why do stripes form in doped antiferromagnets and what is their relationship to superconductivity?”, arXiv:cond-mat/0006071v1.

- [9] S.R. White and D.J. Scalapino, *Phys. Rev. B* **79**, 220504 (2009)
- [10] S.R. White, *Phys. Rev. B* **48**, 10345 (1993)
- [11] S.R. White and D.J. Scalapino, *Phys. Rev. Lett.* **80**, 1272 (1998)
- [12] S.R. White and D.J. Scalapino, *Phys. Rev. Lett.* **81**, 3227 (1998)
- [13] E. Dagotto, J. Riera and D.J. Scalapino, *Phys. Rev. B* **45**, 5744 (1992)
- [14] M. Sigrist, T.M. Rice and F.C. Zhang, *Phys. Rev. B* **49**, 12058 (1994)
- [15] E. Dagotto, *Rev. Mod. Phys.* **66**, 763 (1994)
- [16] S.R. White and D.J. Scalapino, *Phys. Rev. B* **60**, R753 (1999)
- [17] K.-Y. Yang, W.-Q. Chen, T.M. Rice, M. Sigrist, F.-C. Zhang, *New J. Phys.* **11**, 055053 (2009)
- [18] S.-C. Zhang, *J. Phys. Chem. Solids* **59**, 1774 (1998)
- [19] A. Himeda, T. Kato and M. Ogata, *Phys. Rev. Lett.* **88**, 117001 (2002)
- [20] E. Berg, E. Fradkin, and S.A. Kivelson, *Phys. Rev. B* **79**, 064515 (2009);
E. Berg, E. Fradkin, S.A. Kivelson, J. Tranquada, *New J. Phys.* **11**,
115004 (2009); E. Berg, E. Fradkin, E.-A. Kim, S.A. Kivelson, V.
Oganesyan, J.M. Tranquada, and S.C. Zhang, *Phys. Rev. Lett.* **99**,
127003 (2007)
- [21] F. Loder, S. Graser, A.P. Kampf, and T. Kopp, *Phys. Rev. Lett.* **107**,
187001 (2011)

- [22] S. Rommer, S.R. White, and D.J. Scalapino, *Phys. Rev. B* **61**, 13424 (2000)
- [23] V.J. Emery, S.A. Kivelson and H.Q. Lin, *Phys. Rev. Lett.* **64**, 475 (1990)
- [24] C.S. Hellberg and E. Manousakis, *Phys. Rev. Lett.* **78**, 4609 (1997)
- [25] M. Calandra, F. Becca and S. Sorella, *Phys. Rev. Lett.* **81**, 5185 (1998)
- [26] W.O. Putikka, M.V. Luchini and T.M. Rice, *Phys. Rev. Lett.* **68**, 538 (1992)
- [27] S.R. White and D.J. Scalapino, *Phys. Rev. B* **55**, 6504 (1997)
- [28] D.J. Scalapino and S.A. Trugman, *Philosophical Magazine B* **74**, 607 (1996)
- [29] E.W. Carlson, V.J. Emery, S.A. Kivelson, and D. Orgad, “Concepts in High Temperature Superconductivity,” in *The Physics of Conventional and Unconventional Superconductors*, Vol. 2, ed. K.H. Bennemann and J.B. Ketterson (Springer-Verlag 2004)
- [30] D. Poilblanc, *Phys. Rev. B* **49**, 1477 (1994)
- [31] S.R. White and D.J. Scalapino, *Phys. Rev. Lett.* **91**, 136403 (2003)
- [32] G. Hager, G. Wellein, E. Jeckelmann and H. Fehske, *Phys. Rev. B* **71**, 75108 (2005)
- [33] T. A. Maier, G. Alvarez, M. Summers, and T. C. Schulthess, *Phys. Rev. Lett.* **104**, 247001 (2010).

- [34] H.E. Mohottala et al., *Nature Materials* **5**, 377 (2006)
- [35] Y.S. Lee et al., *Phys. Rev. B* **60**, 3643 (1999)
- [36] Q. Li, M. Huecker, G.D. Gu, A.M. Tsvelik, J.M. Tranquada, *Phys. Rev. Lett.* **99**, 067001 (2007); J.M. Tranquada, G.D. Gu, M. Huecker, Q. Jie, H.-J. Kang, R. Klingeler, Q. Li, N. Tristan, J.S. Wen, G.Y. Xu, Z.J. Xu, J. Zhou, M.V. Zimmermann, *Phys. Rev. B* **78**, 174529 (2008)



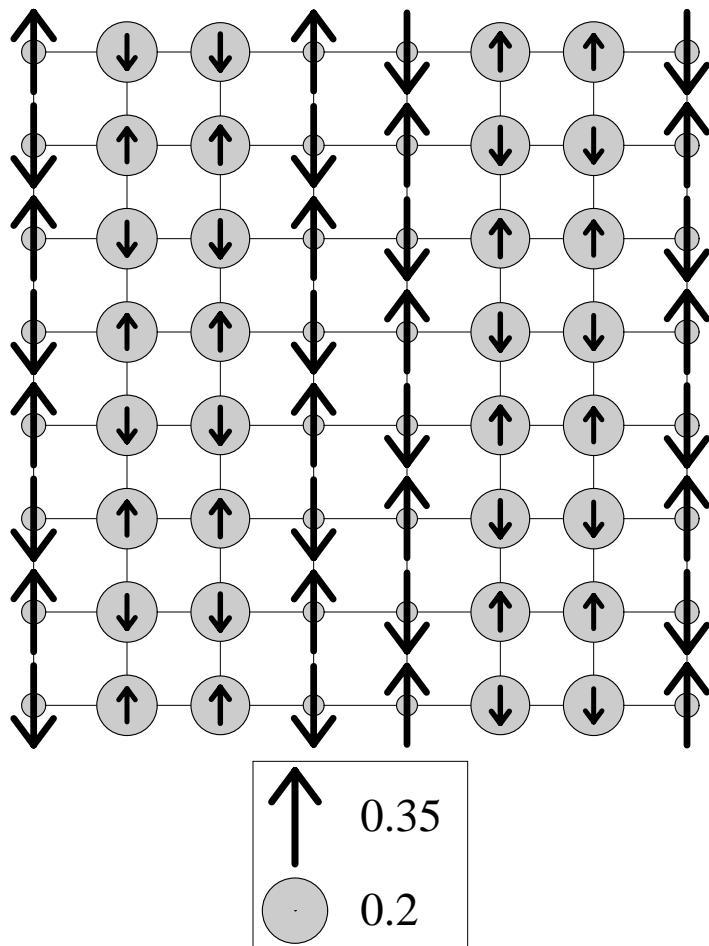


Fig. 1(b)
White and Scalapino